scientific reports

Check for updates

OPEN

Research on the heat transfer characteristics of evaporator tubes in micro turbine engines based on biomimetic parallel leaf vein structure

Qingyu Zhang[1,2], Xinming Zhang[1,3,4]✉, Jing Hu[1]✉ & Guowei Li[1]

This article focuses on optimizing the evaporation and atomization performance of the evaporator tube in the combustion chamber of a microturbine engine, and examines its impact on engine thrust. Given that the evaporator tube design is crucial for enhancing combustion efficiency as a key component of the combustion chamber, this study introduces an innovative evaporator tube structure that incorporates biomimetic design principles through theoretical exploration. The proposed structure adds specifically sized grooves to the inner wall of traditional evaporation tubes to improve the evaporation and atomization processes of fuel droplets. The effectiveness of this design is demonstrated by comparing and analyzing the differences in evaporation and atomization characteristics between traditional and biomimetic evaporation tubes. As the incoming air temperature increases, the diameter of fuel droplets decreases, while the evaporation rate significantly rises. Moreover, when the biomimetic tube's inner wall grooves are precisely designed with a width of 0.5 mm, a depth of 0.6 mm, and a length of 1.5 mm, the atomization effect of fuel droplets reaches its optimal state, significantly improving the evaporation rate compared to traditional evaporation tubes.

Keywords Bionics, Micro turbine engine, Evaporator tube, Parallel leaf vein groove, Atomization

List of symbols

ρ	(fluid density) (Kg/m^3)
ρ	(pressure) (pa)
v	the kinematic viscosity of the fluid) (m^2/s)
U_i	the velocity component in the i-direction) (m/s)
u, v, w	(components of velocity in the x, y, z directions)
a	(heat diffusion coefficient)
t	(fluid temperature) (K)

In recent years, driven by the continuous advancement of global defense technology and the rapid growth of the civil economy, technological innovation in the aviation sector has accelerated—particularly in the development of micro-scale devices, which has become a key focus in both military strategy and the civil UAV industry[1–5]. Among these innovations, the Micro Turbine Engine (MTE) is playing an increasingly vital role in high-end systems such as UAVs, owing to its compact structure, small size, high energy density, and superior thrust-to-weight ratio[6–8].

In the military domain, MTEs are widely deployed across various UAV platforms. Reconnaissance UAVs leverage their compact size and high mobility to execute high-risk intelligence missions deep within hostile territory, while attack UAVs exploit the high power output of MTEs to deliver precise strikes, thereby greatly enhancing operational efficiency and tactical flexibility. In the civilian sector, MTEs also exhibit broad application

[1]College of Mechanical and Electrical Engineering, Changchun University of Science and Technology, Changchun 130022, China. [2]College of Control Science and Engineering, Bohai University, Jinzhou 121013, China. [3]School of Mechatronic Engineering and Automation, Foshan University, Foshan 528225, China. [4]Precision Machining and Special Machining Innovation Team, Guangdong Education Department, Foshan 528225, China. ✉email: zxmcust163@163.com; hujing@cust.edu.cn

potential. In logistics and distribution, MTE-powered UAVs can efficiently perform transport tasks in remote or complex terrains; in agricultural plant protection, UAVs equipped with MTEs enable large-scale, precise pesticide application, improving both efficiency and crop quality. This rapidly advancing technological trend has garnered growing attention from the global academic community, and MTE research is increasingly recognized as a prominent focus in current scientific exploration[9,10].

In MTE systems, the combustion chamber, as a core component, plays a pivotal role in determining overall engine performance. Common structural types include single-tube, ring-tube, and annular chambers, which can be further categorized by airflow pattern into straight-flow, folded-flow, and reverse-flow configurations[11]. Among these, the straight-flow combustion chamber has become the mainstream choice due to its effective flow field organization and high combustion efficiency[12]. It optimizes airflow distribution and enhances fuel–air mixing, thereby improving combustion efficiency and reducing pollutant emissions. However, under complex operating conditions—such as high temperature, high pressure, and rapid load fluctuations—straight-flow chambers still face technical challenges, including unstable combustion and difficult emission control, highlighting the urgent need for improved adaptability and stability[13–15].

In recent years, bionic structural design has opened a new avenue for optimizing combustion chamber performance. By emulating the efficient forms and functional mechanisms found in nature, bionic designs have demonstrated clear advantages in enhancing combustion efficiency and flow control. For instance, the incorporation of bionic vortex generators and drag-reducing coatings can significantly improve airflow organization and fuel–air mixing, thereby reducing energy consumption and emissions. Moreover, bionic structures hold strong potential for dynamic regulation, intelligent response, and system miniaturization in aircraft engines, industrial gas turbines, and distributed energy systems. Despite current challenges—such as complex fabrication processes, high costs, and concerns over long-term operational stability—ongoing advances in materials science, manufacturing technologies, and computational simulation are expected to accelerate the practical application of bionic structures in combustion chambers, offering substantial technical and practical benefits.

Given the stringent requirements of the MTE for compactness and system reliability, the evaporator tube—a critical component—must achieve efficient fuel atomization and evaporation within a limited space[16]. However, traditional evaporator tube designs typically feature simple structures, low atomization efficiency, and inadequate fuel–air mixing, resulting in incomplete combustion and reduced overall engine performance. Additionally, the limited evaporation surface area constrains the fuel's evaporation rate and efficiency, making it difficult to meet the demands of high-load operation. Furthermore, traditional tubes often lack sufficient durability in high-temperature and corrosive environments, leading to material degradation that significantly undermines system reliability and service life.

In recent years, advances in materials science, flow control strategies, and advanced manufacturing technologies have created new opportunities for the structural optimization of evaporator tubes. The use of heat- and corrosion-resistant materials has significantly enhanced their thermal stability and structural integrity, thereby improving combustion efficiency and expanding the operational envelope. However, several technical challenges remain to be addressed. First, the fabrication of micron- and nano-scale structures, combined with the need for high-precision manufacturing, has led to increased production costs and longer delivery cycles, hindering large-scale deployment. Second, the extreme working conditions of the MTE involve complex multi-physical field coupling, posing greater challenges for system control. Third, although intelligent monitoring systems are evolving, their long-term reliability and data processing accuracy still require further validation. Fourth, the high cost of system integration continues to be a major barrier to widespread adoption. Therefore, advancing interdisciplinary innovation—in materials science, structural engineering, fluid dynamics, monitoring technologies, and cost-performance optimization—is essential for the future development of this technology.

To address the limitations of traditional evaporator tubes in fuel atomization and evaporation efficiency, this study proposes a novel structure inspired by bionic design principles. By systematically analyzing the coupling relationship between structural morphology, flow characteristics, and atomization behavior, the key structural factors influencing atomization and evaporation are identified and evaluated. This research not only introduces innovative strategies for optimizing fuel management within the evaporator tube but also establishes a theoretical foundation for the design of high-efficiency combustion chambers and the enhancement of the MTE combustion performance, offering significant potential for engineering applications.

Design of a new type of evaporator tube based on biomimetics

Evaporator tube designs typically include three basic forms: straight tube, L-shaped turning, and U-shaped surround. Each form plays a distinct role in fuel atomization and evaporation, tailored to different application scenarios and needs, as shown in Fig. 1, Supplementary information. These designs not only highlight the diversity of evaporator tube structures but also demonstrate the strong link between their form and function, each contributing uniquely to efficient atomization and deep evaporation of fuel. The structural characteristics and practical advantages of different evaporator tube designs are comprehensively summarized in Table 1, offering both scientific insights and practical guidance for selecting and designing evaporator tubes. By choosing the most suitable design based on specific needs, optimal fuel atomization and evaporation effects can be achieved. The detailed characteristics and applications of each evaporator tube structure are presented in Table 1.

Although various evaporator tube structures—whether straight, L-shaped, or more complex forms—can demonstrate similar functional efficiency in the evaporation process, their differences become more pronounced when optimizing for layout aesthetics and fluid dynamics. Among them, the straight tube structure, with its unmatched advantages, has emerged as the preferred choice in many practical applications, especially at intermediate frequencies, making it the top selection for designers and engineers. The preference for the straight tube structure is primarily due to its simplicity and spatial efficiency: its straight-line form is not only visually

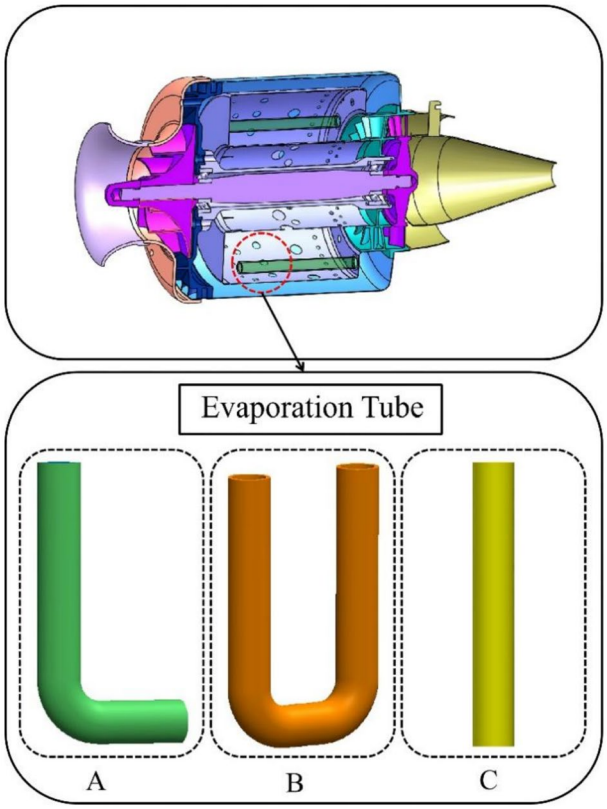

Fig. 1. Physical picture of common evaporator tubes[17]. (**A**) Model diagram of L-shaped evaporator tube, (**B**) Model diagram of U-shaped evaporator tube, (**C**) Model diagram of straight evaporator tube.

Type	Characteristic	Application
Straight tube type	Simple structure, direct fluid flow path, relatively small pressure loss	Suitable for situations where low fuel flow resistance is required and the spatial layout allows for straight line arrangement, it is beneficial for stable fuel flow and initial atomization inside the tube
L-type	By introducing a 90 degree or near 90 degree inflection point, changing the direction of fuel flow may generate a vortex effect, promoting the mixing of fuel and air	Suitable for scenarios that require the use of vortices at turning points to enhance fuel atomization, especially for achieving efficient fuel atomization in compact spaces
U-shaped	Forming a semi-circular circuit increases the residence time and path length of fuel in the tube, which is beneficial for the full preheating and evaporation of fuel	Suitable for situations where it is necessary to extend the contact time between fuel and heat source and improve evaporation efficiency, commonly used in systems that require high preheating or fine adjustment of fuel state

Table 1. Characteristics and applications of different evaporator tube structures.

appealing but also maximizes efficiency in a compact space, making it a model in design. Straight tube evaporator tubes stand out because of their direct and efficient connection characteristics, which further enhance their performance. The straight tube design enables a simple connection between the evaporator tube and the fuel nozzle, eliminating the need for complex tubing layouts and additional connectors. This feature greatly simplifies the manufacturing process and maintenance, while significantly reducing design, assembly time, and costs.

For MTE, controlling pressure loss is crucial for ensuring efficient operation. The straight tube design offers a smooth combustion fluid path, avoiding complex bends and branches. This effectively reduces resistance and energy dissipation during flow, ensuring low pressure loss and providing a strong foundation for the efficient and stable operation of the engine. Additionally, shortening the residence time of fuel in the MTE evaporator tube is critical for enhancing the evaporation rate and stability of fuel transfer. To achieve this, a compact design was implemented for the straight tube structure, effectively reducing the fuel flow time by optimizing the tube length. In contrast to more complex, tortuous designs, this linear configuration significantly minimizes the risk of fluctuations and uneven evaporation during fuel retention, further improving the efficiency and stability of fuel transmission[18]. To further optimize the evaporation performance and fuel atomization of the straight tube structure, a parallel leaf vein-shaped reinforcement was innovatively introduced inside the tube. Inspired by natural veins, this design significantly enhances the fuel evaporation rate and improves combustion stability and efficiency by finely regulating fluid dynamics within the combustion chamber. This innovation injects new energy into the high-performance output of MTEs. With these advancements, the straight tube structure's

leading position in evaporator tube technology is further solidified, offering an optimal solution for creating efficient, compact, and reliable energy conversion systems.

Selection of biomimetic prototypes

The inspiration for leaf veins comes from the field of bionics. With technological advancements and innovation, leaf vein structures have undergone significant transformation, becoming an essential component in modern aviation composite materials[19,20]. The brilliance of these biomimetic designs lies not only in their mimicry of the elegant form of leaves in nature but also in their ingenious integration of nature's wisdom into high-strength, lightweight materials science[21]. In aviation, the application of leaf vein structures has proven its unparalleled superiority. These structures come in various types, including intricate mesh veins that interweave like natural veins, offering strong support and stability for composite materials. There are also simple and aligned parallel veins, which efficiently transmit force and enhance material strength. Additionally, the unique palm-like veins, resembling an unfolded palm, not only add aesthetic appeal but also integrate greater flexibility and adaptability into the structural design[22]. Common leaf vein structures include reticular veins, parallel veins, and palmar veins, as shown in Fig. 2. These structures highlight the boundless possibilities of integrating nature with engineering technology in unique ways. Moreover, the application of leaf vein structures in aviation composite materials has led to significant improvements in performance. These structures not only reduce material weight and lower energy consumption but also significantly enhance the strength, rigidity, and durability of materials. Additionally, the unique morphology of leaf vein structures helps optimize aerodynamic performance, reduce flight resistance, and improve flight efficiency[23]. These advantages make the application of leaf vein structures in aviation increasingly promising, becoming a key driver of technological innovation and development in the industry.

In the design of the evaporator tube's inner wall, the introduction of texture can impact evaporation efficiency in several ways: (1) Increasing Surface Area: Texture design can enhance the surface area of the inner wall, providing more area for evaporation. A larger surface area allows more water to evaporate simultaneously, improving evaporation efficiency. (2) Promoting Liquid Distribution: Properly designed textures can promote the uniform distribution of liquid across the inner wall, preventing local liquid accumulation. This helps improve evaporation efficiency, as liquid buildup can slow the evaporation rate. (3) Enhanced Capillary Action: Specific texture designs, such as microporous structures, can enhance capillary action, facilitating the adsorption of liquids onto the inner wall of the evaporator tube and keeping them at the evaporation interface. This ensures a high evaporation rate, as droplets are continuously transported to the interface. Furthermore, certain features from the texture of duckweed, such as mesh patterns or porous structures, can be adapted and integrated with the actual requirements of the evaporator tube to innovatively improve evaporation efficiency.

Compared to straight tube structures, especially those incorporating leaf vein reinforcement design, other forms of evaporator tubes, such as U-shaped and L-shaped, may face two major challenges in certain application scenarios[24,25]: (1) Layout Complexity and Cost Escalation: The design of these non-linear evaporator tubes often involves more complex tubing layouts with additional connection nodes and branch structures. This significantly increases manufacturing and assembly complexity, raising costs. Furthermore, multiple bends and connections can introduce additional pressure losses and increase fluid dynamic resistance, negatively impacting the overall performance of the evaporator tube. (2) Restricted Heat Transfer Efficiency: Compared to vein-shaped reinforced straight tubes, U-shaped and L-shaped evaporator tubes have relatively smaller specific surface areas, limiting their heat transfer efficiency. This difference in heat transfer performance directly impacts the evaporation rate of

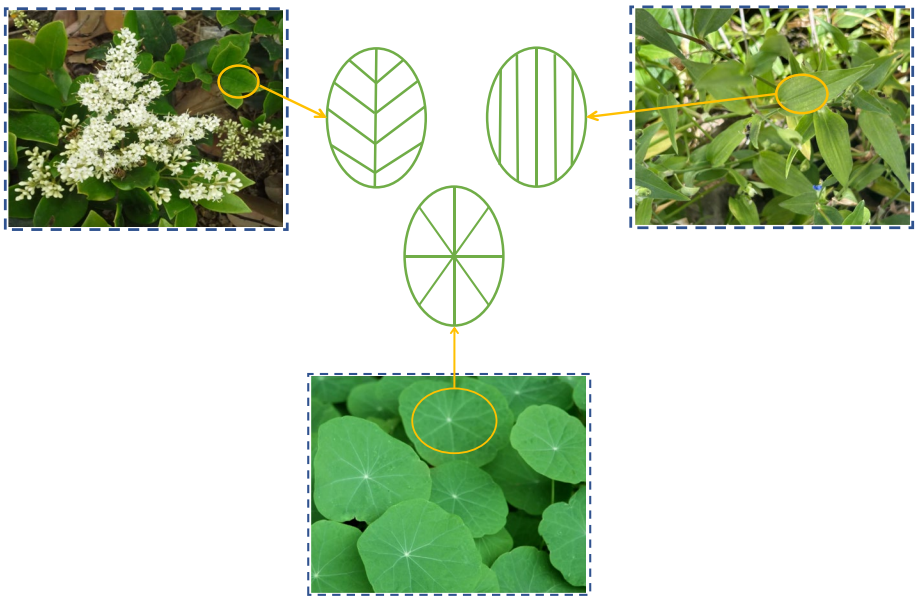

Fig. 2. Common leaf vein structures.

the evaporator tube and the overall system efficiency, thereby constraining the performance of the entire energy conversion system.

In summary, introducing texture in the design of evaporator tubes effectively enhances evaporation efficiency by increasing surface area, promoting uniform liquid distribution, and boosting capillary action. However, compared to straight tube structures with leaf vein reinforcement designs, non-linear evaporator tubes, such as U-shaped and L-shaped, face challenges such as complex layouts, higher costs, and limited heat transfer efficiency in practical applications. These issues not only increase manufacturing and assembly complexity but may also lead to additional pressure losses and fluid dynamic resistance due to the intricate tubing layout, negatively impacting the overall performance of the evaporator tube and the efficiency of the entire energy conversion system. Therefore, in the design and innovation of evaporator tubes, it is essential to comprehensively consider the advantages and disadvantages of different forms and optimize them based on actual needs to achieve the best evaporation efficiency and system performance. Ultimately, the design integrating a parallel leaf vein structure with straight evaporator tubes proves to be a promising and effective solution. A new type of evaporator tube structure, incorporating this design, is shown in Fig. 3.

Analysis of influencing factors on the design of parallel leaf veins in wall grooves

In designing the inner wall of the evaporator tube, a parallel leaf vein structure is chosen over mesh or palmate vein patterns primarily to enhance fluid flow and heat transfer efficiency. The term 'parallel veins' refers to grooves aligned along the axial direction of the tube, resembling the parallel vein arrangement in plant leaves. This structure promotes the formation of a stable parallel flow pattern within the tube, thereby improving both heat transfer and fluid flow performance[26,27].

Heat transfer efficiency

(1) Heat Transfer Path: Inside the evaporator tube, heat must transfer from the tube wall to the gas–liquid two-phase flow (typically a liquid or gas–liquid mixture), with the gas–liquid flow then carrying away the heat through evaporation or convection. The design of the parallel leaf vein shape helps enhance this heat transfer by guiding the flow more efficiently along the vein direction, optimizing heat transfer and improving overall evaporation performance. (2) Reduced Thermal Resistance: The parallel leaf vein shape helps reduce thermal resistance because the heat transfer path between the leaf veins is relatively short and direct. This minimizes heat loss during the transfer process, improving overall heat transfer efficiency. (3) Uniform Temperature Distribution: The parallel leaf vein shape promotes a more uniform temperature distribution inside the evaporator tube,

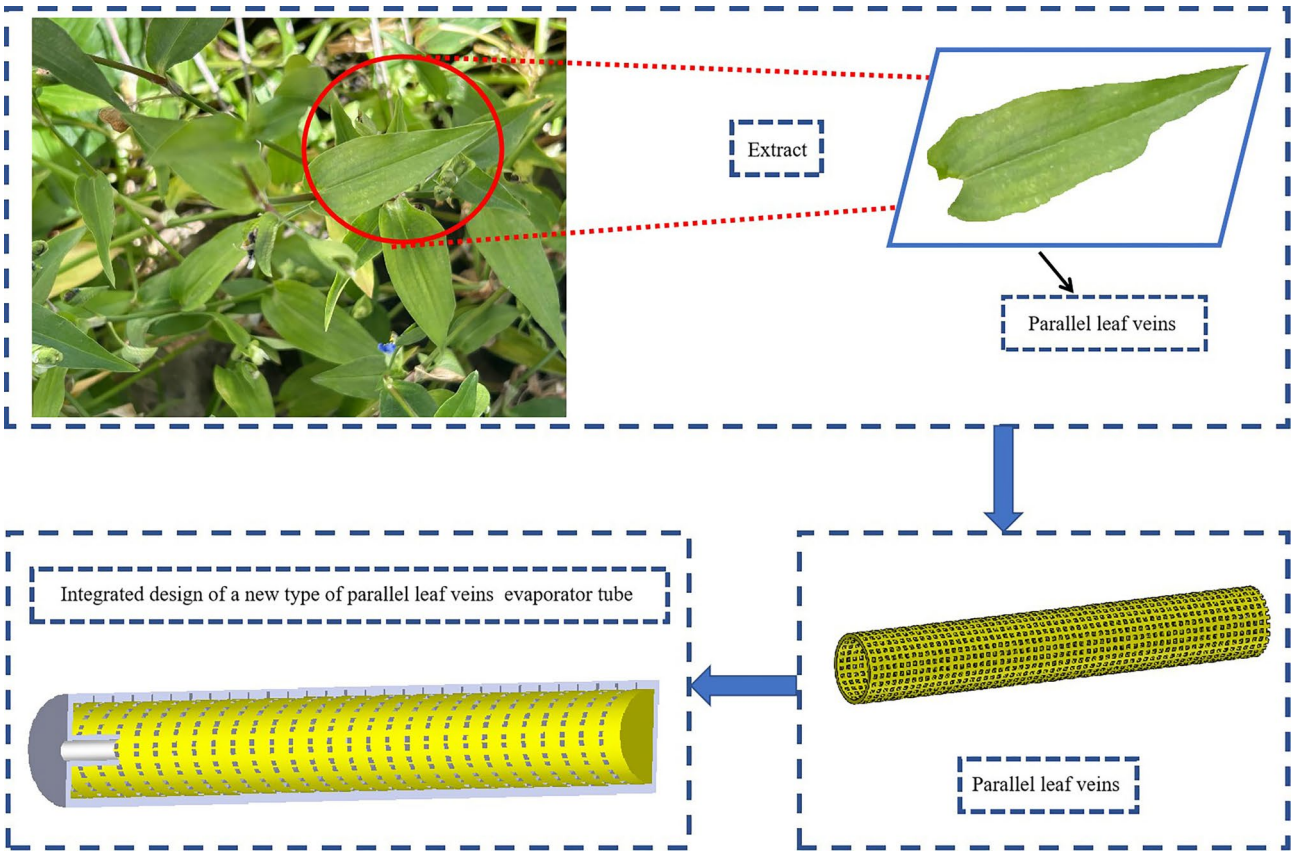

Fig. 3. Schematic diagram of biomimetic parallel leaf vein structure.

enhancing heat transfer efficiency and reducing thermal stress. This leads to more stable and effective operation of the system.

Flow characteristics
(1) Working Fluid Flow Path: The flow path of the working fluid inside the evaporator tube greatly influences heat transfer efficiency. The parallel leaf vein design guides the fluid to flow along the vein direction, effectively utilizing the available space within the tube. (2) Reduced Flow Resistance: Parallel vein shapes have fewer branches and intersections compared to mesh or palm veins, which helps reduce the resistance to fluid flow, improving flow efficiency. (3) Pulsating Flow: In certain evaporator tubes, such as pulsating heat tubes, the pulsating flow of the working fluid plays a key role in heat transfer. The parallel leaf vein design optimizes the characteristics of this pulsating flow, allowing more effective heat transfer between the evaporation and condensation sections.

Other factors
(1) Structural Stability: The parallel leaf vein structure is relatively simple and stable, helping to minimize deformation or damage to the evaporator tube during prolonged use. (2) Manufacturing and Maintenance Costs: The parallel vein design is easier to manufacture and maintain, reducing the overall manufacturing and operational costs of the evaporator tube.

In summary, the choice of a parallel leaf vein shape inside the evaporator tube is primarily driven by its superior heat transfer efficiency and flow characteristics. This design optimizes heat transfer paths, reduces thermal resistance, ensures uniform temperature distribution, minimizes flow resistance, and enhances pulsating flow characteristics. These advantages make the parallel leaf vein shape the preferred design for the interior of evaporator tubes.

To optimize the groove size of the new structure, a combination of orthogonal experimental design and numerical simulation can be employed to identify the optimal dimensions. When exploring the optimal groove size, factors such as element shape, size, and spacing distribution should be adjusted. A systematic study of these variables will help determine the best configuration, enabling the identification of the most suitable structural design rules tailored to specific design needs.

Establishment of heat transfer model inside evaporator tube

The governing equations governing the flow of fluid within an evaporator tube encompass the continuity equation for incompressible flow in three dimensions with constant physical properties, the Navier–Stokes equation for momentum conservation, and the energy conservation Eq. ([28]).

The continuity equation:

$$\frac{\partial u}{\partial x}+\frac{\partial v}{\partial y}+\frac{\partial w}{\partial z}=0 \tag{1}$$

in Eq. (1), u、v、w are the components of velocity in the *x*, *y*, *z* directions, respectively.

Momentum conservation equation:

$$u\frac{\partial U_i}{\partial x}+v\frac{\partial U_i}{\partial y}+w\frac{\partial U_i}{\partial z}=-\frac{1}{\rho}\frac{\partial p}{\partial x}+v\left(\frac{\partial^2 U_i}{\partial x^2}+\frac{\partial^2 U_i}{\partial y^2}+\frac{\partial^2 U_i}{\partial z^2}\right) \tag{2}$$

in Eq. (2): ρ is the fluid density; P is the pressure; v is the kinematic viscosity of the fluid; U_i is the velocity component in the i-direction.。

The energy conservation equation:

$$u\frac{\partial t}{\partial x}+v\frac{\partial t}{\partial y}+w\frac{\partial t}{\partial z}=a\left(\frac{\partial^2 t}{\partial x^2}+\frac{\partial^2 t}{\partial y^2}+\frac{\partial^2 t}{\partial z^2}\right) \tag{3}$$

In Eq. (3): α is the heat diffusion coefficient; *t* is the fluid temperature.

Method of calculation

This study employed the commercial software FLUENT R1 for CFD simulations. The flow field in the evaporator tube was solved using a pressure-based implicit separation solver. The standard k-ε turbulence model was applied, with the near-wall treatment based on the standard wall functions. The pressure–velocity coupling was handled using the SIMPLE algorithm, and the remaining equations were discretized using a second-order upwind scheme The nozzle atomization was modeled using the DPM (Discrete Phase Model), with the secondary fragmentation process modeled by the Wave model and the collision process represented by the Stochastic Collision model. The internal temperature distribution of a single droplet was assumed using the zero model. To simulate the changes in gas-phase composition during the evaporation process, a component transport model was implemented, where a single component, $C_{12}H_{23}$, was used as a simplified replacement for the complex aviation kerosene.

The simulation is conducted under steady-state conditions, with a convergence criterion defined by residuals falling below 1×10^{-5}. Additionally, the velocity field is monitored throughout the calculation to ensure solution stability. For wall boundary conditions, no-slip conditions were applied, and standard wall functions were used to handle near-wall effects. For droplets colliding with the wall, the Lagrangian Wall Film model was employed.

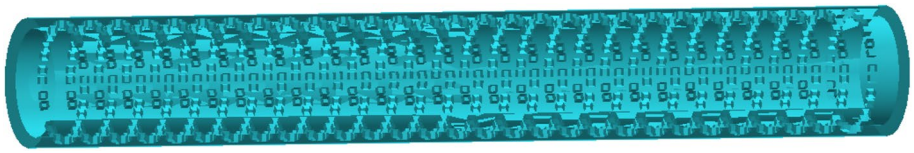

Fig. 4. Geometric model of the target.

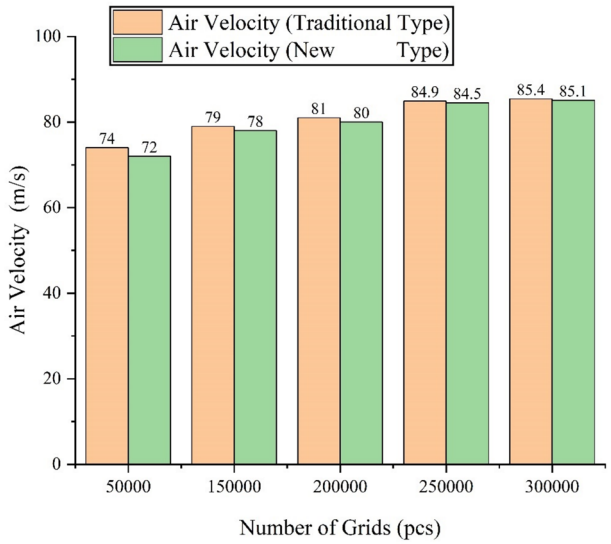

Fig. 5. Verification of the independence between the number of traditional evaporator tube grids and the number of new evaporator tube grids.

In this simulation, the impact of the external environment on fuel atomization and evaporation inside the evaporator tube was neglected, and the wall was treated as adiabatic to simplify the boundary conditions further.

Verification of physical model and grid independence

Based on existing relevant data models, the structure of a single evaporator tube was first extracted, then modified and optimized to create a target geometric model suitable for numerical simulation analysis, as shown in Fig. 4. A non-structured mesh partitioning method was employed for the numerical simulations. During the grid partitioning process, local mesh refinement was applied at the nozzle outlet, regions with significant structural changes, and the tube wall surface. To ensure the accuracy of the results, grid independence validation was performed.

The comparison of grid divisions in the model shown in Fig. 5 demonstrates that when the number of grid cells for traditional evaporator tubes is around 2.5 million and for the new evaporator tube network is approximately 2.2 million, the relatively optimal solution is achieved by utilizing the evaporator tubes MTE.

Boundary conditions and research plan

Boundary condition

The air inlet is defined as a mass flow inlet with a temperature of 465 K. To more accurately represent the development of turbulence, the inlet turbulence boundary conditions are specified with a turbulence intensity (TI) of 5% and a hydraulic diameter (HD) of 5 mm. The outlet boundary is set as a pressure-free outflow condition, allowing gas to exit the domain naturally without the imposition of additional pressure constraints. For wall boundaries, a stationary no-slip condition is applied to all solid surfaces.

Comparison of evaporator tube performance under different structural states

To investigate the impact of shape and size parameters of parallel leaf veins on the performance of evaporator tubes, the Design and Analysis of Experiments (DAE) method was utilized. To reduce the number of numerical simulation experiments and ensure more reliable analysis results, the orthogonal experimental method was chosen to perform numerical simulations on a straight evaporator tube with parallel leaf veins. A total of 9 schemes were designed based on the L_9 (3^4) orthogonal table. Three groove shape control parameters were selected as influencing factors, with three levels for each factor. The resulting scheme is shown in Table 2. Here, A represents the depth of the groove on the tube wall, B represents the width of the groove, and C represents the length of the groove. A1 corresponds to the depth of the groove of 0.5 mm, A2 to the depth of the groove of

Programmatic	A	B	C	Depth(mm)	Width(mm)	Length (mm)
a	1	1	1	0.5	0.5	0.5
b	1	2	2	0.5	1	1
c	1	3	3	0.5	1.5	1.5
d	2	1	2	0.55	0.5	1
e	2	2	3	0.55	1	1.5
f	2	3	1	0.55	1.5	0.5
g	3	1	3	0.6	0.5	1.5
h	3	2	1	0.6	1	0.5
i	3	3	2	0.6	1.5	1

Table 2. Design table for shape control factor test scheme.

Programmatic	Evaporation rate(%)	Outlet SMD (μm)	Air flow (g/s)	Average outlet temperature(K)
a	18.01	45.46	2.554	532.47
b	3.01	36.51	2.552	530.43
c	3.92	30.94	2.556	530.11
d	6.79	38.86	2.554	530.59
e	2.37	35.39	2.554	531.21
f	2.50	40.69	2.555	528.98
g	23.98	29.52	2.551	539.93
h	2.58	33.66	2.555	529.19
i	5.20	39.81	2.552	534.64

Table 3. Calculation results of evaporator tubes for each program.

0.55 mm, and so on. For Scheme A, the influencing factors are A1B1C1, which corresponds to the depth of the groove 0.5 mm, the width of the groove 0.5 mm, and the length of the groove 0.5 mm.

The calculation results for the 9 different schemes for evaporator tubes are presented in Table 3. The analysis reveals that the evaporation rates of schemes A, D, and G are relatively high, while the airflow rate is lower and the average outlet temperature is higher. No significant correlation was observed in terms of factors related to the average diameter of the sotel. Among these three schemes, the inner wall width of the groove tube remains the same, while the depth of the groove and thickness vary, indicating that the inner wall width is a key factor influencing the evaporation rate. The data suggests that a smaller the width of the groove leads to greater evaporation of liquid droplets inside the tube and higher turbulence levels in the flow field, which are favorable for the atomization and evaporation of liquid droplets.

Result analysis

Selection of feature surfaces

When studying the influence of evaporator tube and inflow characteristic parameters on the fuel atomization and evaporation performance inside the evaporator tube, the middle section is selected for analysis. The specific location of this section is shown in Fig. 6.

The parameters analyzed in this study mainly include the Sauter mean diameter (SMD) of fuel droplets and the fuel evaporation rate. The SMD of droplets can be directly extracted from the numerical simulation software to obtain the value at each cross-section. For the fuel evaporation rate, the amount of fuel evaporated at each section is calculated from the numerical simulation. The evaporation rate is then determined as the ratio of the evaporated fuel to the total fuel amount, allowing for the calculation of the fuel evaporation rate at each section.

The influence of parallel leaf veins on the air temperature inside the evaporator tube

These nine structural variations significantly influence the heat transfer pathways within the evaporator tube and the fuel's evaporation behavior by altering the depth of the groove, the width of the groove, and the length of the groove. Overall, the groove dimensions determine the local heat concentration capacity, the degree of airflow disturbance, and the axial extent of the high-temperature zone, thereby directly affecting evaporation efficiency. Specifically, the depth of the groove controls the intensity of heat concentration near the wall—deeper grooves are more favorable for forming localized evaporation hot spots. The width of the groove affects the distribution of fuel and airflow, as well as the smoothness of the main flow region. The length of the groove governs the axial extension of the high-temperature zone, which helps prolong the residence time of droplets in high-temperature regions, enhancing heat transfer and promoting more complete evaporation.

In the temperature cloud map at the intermediate interface shown in Fig. 7, distinct differences in heat transfer performance are observed among the various schemes. Scheme g (0.6 mm depth, 0.5 mm width, 1.5 mm

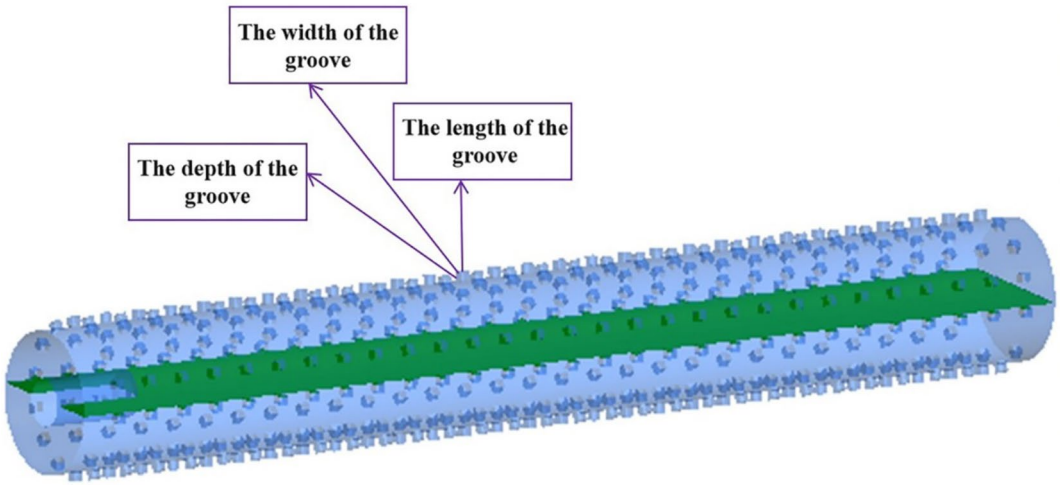

Fig. 6. Position of the middle section relative to the evaporator tube.

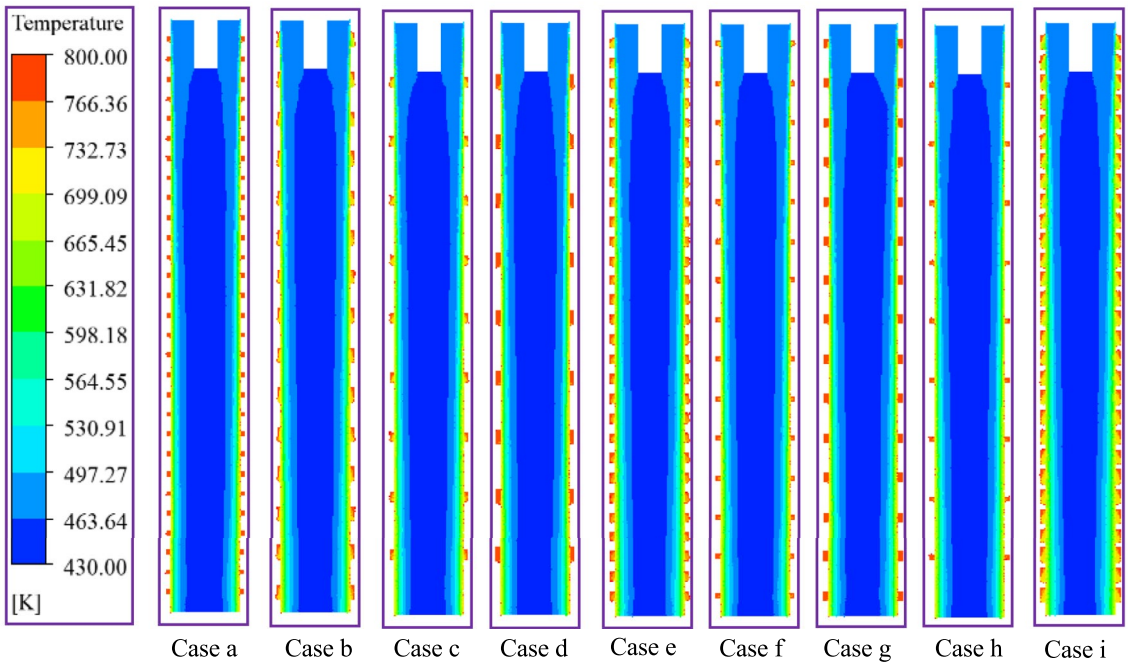

Fig. 7. Temperature cloud map of the middle section of the evaporator tube.

length) demonstrates the best overall performance, forming an extensive red high-temperature zone near the tube wall and effectively extending the thermal field toward the center of the tube. This indicates that the groove structure not only enhances heat transfer efficiency at the wall surface but also improves the distribution of high-temperature radiation toward the central region, creating a favorable microenvironment that promotes the rapid evaporation of fuel droplets.

In addition, scheme g exhibits a relatively smooth temperature gradient, indicating continuous and uniform heat distribution. This helps prevent localized overheating and enhances the overall thermal stability of the system. In contrast, scheme a (0.5 mm depth / 0.5 mm width / 0.5 mm length), with its shallow and short grooves, results in limited heat concentration, a very small high-temperature region, and low heat transfer efficiency. Scheme i (0.6 mm depth / 1.5 mm width / 1 mm length) features larger grooves, but the heat tends to concentrate excessively in localized areas, leading to the formation of hot spots. These hot spots can trigger airflow instability or heat recirculation, potentially disrupting uniform fuel distribution and negatively affecting the overall evaporation performance.

In summary, scheme g represents an optimized structural configuration, combining moderate the depth of the groove, appropriate width, and sufficient length extension. This design not only enables the effective formation

and uniform distribution of the high-temperature zone but also demonstrates excellent heat conduction and overall thermal stability. It stands out as the optimal solution among the current thermally optimized structural designs.

The influence of parallel leaf veins on the air velocity inside the evaporator tube

Figure 8 illustrates the airflow velocity distribution inside the evaporator tubes with different structures, highlighting the significant impact of the notch design on airflow perturbation, shear variation, and atomization dynamics. Among all tested scenarios, scenario g exhibits the optimal flow state: the velocity in the main flow region remains high, while beneficial localized perturbations form in the notch region. These perturbations do not cause significant reflux and enhance the relative motion between the airflow and liquid droplets. The increased relative velocity boosts shear force, accelerating both primary droplet fragmentation and secondary atomization.

In contrast, schemes a, d, and h exhibit minimal interference with the main airflow due to the insufficient length or depth of the grooves. The turbulence intensity is weak, leading to inadequate relative gas–liquid motion and larger atomized particle sizes, which hinder the complete evaporation of fuel. On the other hand, schemes c, f and i despite having larger notches, experience velocity attenuation in certain areas, even forming low-speed reflux zones, which in turn reduce the efficiency of mass and heat transfer. The notch configuration in scheme g effectively prevents velocity destabilization, maintains the main flow, and enhances turbulence, thereby significantly improving the efficiency of airflow-droplet interaction without notably increasing flow resistance.

The influence of parallel leaf veins on the atomization and evaporation of fuel droplets

Figure 9 presents the temperature distribution and trajectories of fuel droplets within nine different novel evaporator tube structures. At the initial stage of injection, fuel droplets typically exhibit low temperatures. Over time, they gradually absorb ambient heat, leading to an increase in temperature, evaporation, and eventual atomization. Concurrently, the droplet diameter decreases, and the droplets undergo collisions and diffusion within the tube. As shown in the figure, the droplet temperature along the axial direction of the evaporator tube progressively increases, while droplets moving near the tube wall tend to exhibit higher temperatures. Under the influence of cyclonic airflow, the droplets continue to diffuse, displaying complex yet organized trajectories. This process is influenced not only by the changing thermophysical properties of the droplets but also by the flow field structure within the evaporator tube. Figure 9 thus offers an intuitive and valuable basis for further understanding the evaporation and atomization behavior of fuel droplets.

In order to further investigate the influence mechanism of notch length, width and depth on the evaporation rate and atomization uniformity of fuel droplets, this paper systematically compares the temperature distribution and flow field characteristics under different notch dimensions (combined length, width and depth) based on different evaporator tube structures shown in Fig. 9.

Figure 9 illustrates the particle trajectory distribution and temperature evolution inside the evaporator tube, providing key insights into the droplet heat path and atomization behavior. The particle trajectories show that, in the g-scheme, droplets are guided and perturbed by the grooves, with their paths bringing them closer to the

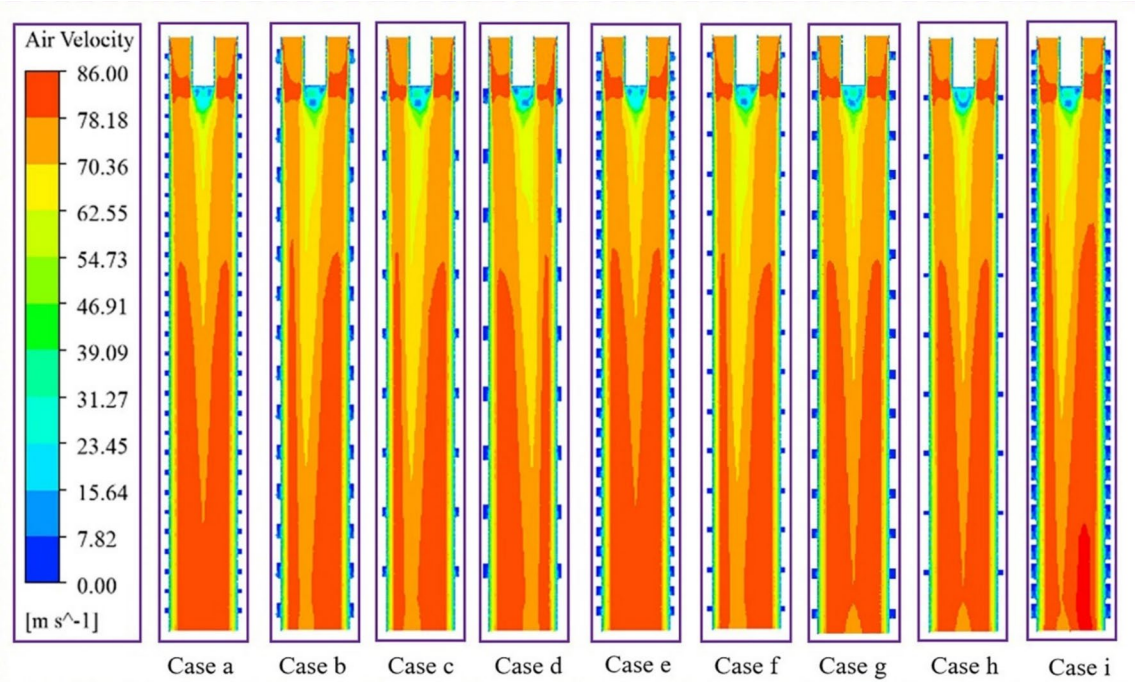

Fig. 8. Temperature cloud map of the middle section of the evaporator tube.

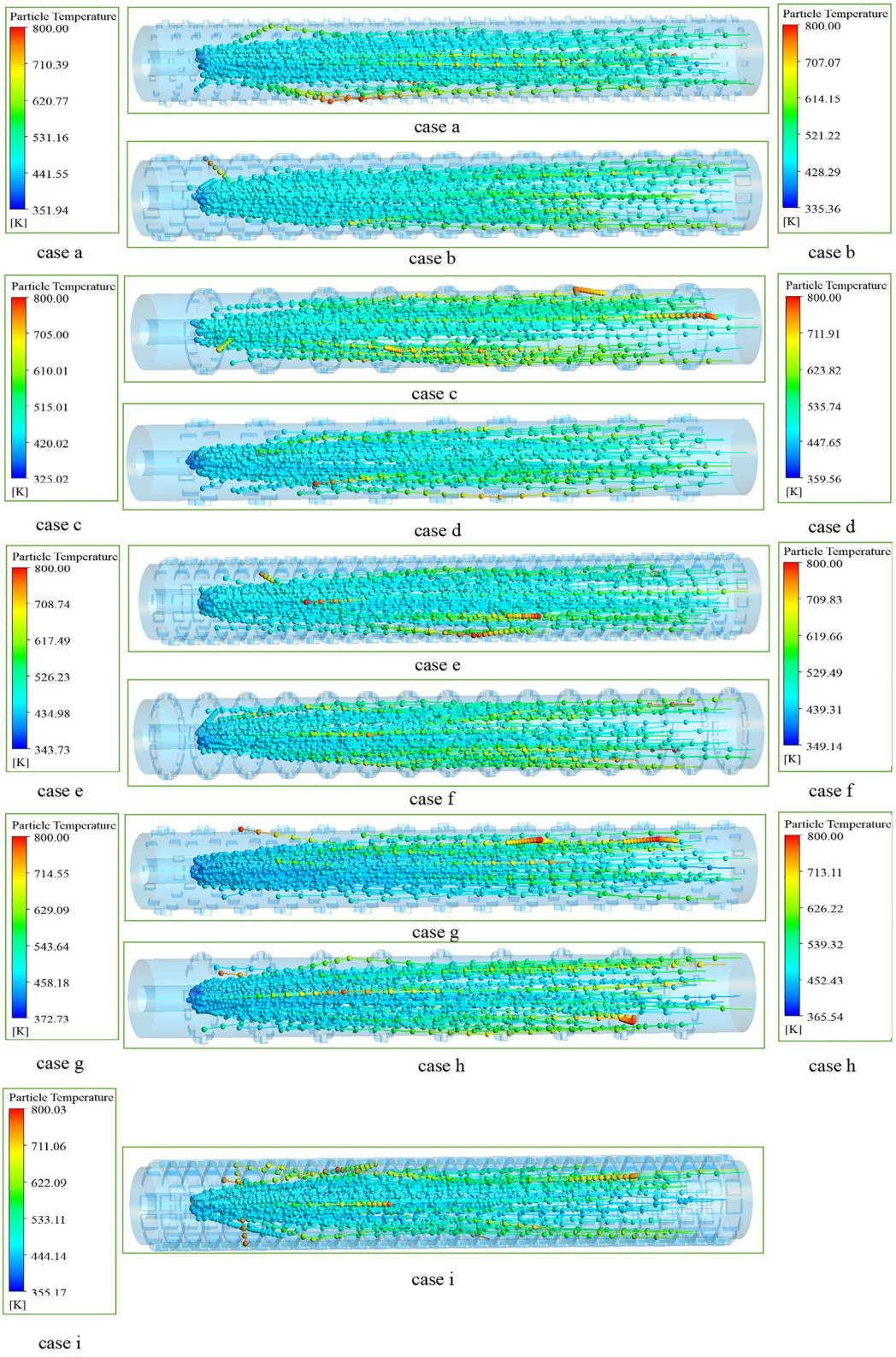

Fig. 9. Comparison of fuel droplet temperature distribution.

high-temperature region of the tube wall. The overall distribution is more uniform, and the temperature rise rate is faster. This indicates that the structure not only effectively extends the droplets' residence time in the high-temperature region but also increases their contact frequency with both the hot wall and hot air, significantly enhancing heat transfer efficiency.

Further observation reveals that the particle temperature profile in scheme g increases sharply, indicating fast heat exchange and a higher likelihood of droplets reaching the evaporation point. In contrast, the particle temperature rises more slowly in schemes a and d, with trajectories concentrated in the low-temperature zone at the center of the tube. This suggests that the grooves' ability to guide and perturb the droplets is insufficient. Although the particle distribution in schemes c and i is broader, they tend to form local pile-ups or disordered trajectories in the grooves, disrupting the consistency of atomization. Overall, the g structure optimizes heat exchange by controlling the depth and length of the grooves, achieving fast heating, uniform distribution, and smaller atomized particle sizes. It is the most balanced scheme in terms of structure and thermodynamic performance.

As the fuel droplets continue to move under the influence of cyclonic airflow, their trajectories become increasingly complex. This complexity enhances the mixing, collision, and fragmentation effects between the droplets and the airflow, further refining the droplet size distribution. The size of the notch also significantly impacts the development of the cyclone. Smaller notches restrict the formation and development of the cyclone, hindering effective diffusion and atomization. Conversely, excessively large notches may lead to cyclone instability, disrupting droplet trajectories. Only when the notch size is optimal can the cyclone and groove structure effectively couple, forming a stable and efficient flow field.

Orthogonal experimental analysis

Using the orthogonal analysis method, the evaporation rate is treated as a single indicator. The orthogonal analysis table is shown in Table 4. The three values in rows K1, K2, and K3 represent the sum of the evaporation rates corresponding to the first, second, and third levels of factors A, B, and C, respectively. The values in rows k1, k2, and k3 are the averages of the corresponding K1, K2, and K3 values, i.e., k1 = K1/3. The range is calculated as the absolute difference between the maximum and minimum of the three values k1, k2, and k3 in each column. The larger the range, the greater the impact of that factor on the evaporation rate. The column with the largest range corresponds to the key factor that most significantly influences the evaporation rate.

From the table, it can be analyzed that the order of the impact of each influencing factor on the evaporation rate, from smallest to largest, is as follows: C (length), A (depth), and B (width). The grooves on the inner wall of the tube have relatively deep depths, and the longer the height and length, the more conducive it is to improving the evaporation rate, although this also increases air flow resistance. The minimum difference in the length of the grooves inside the evaporator tube is 5.09, which indicates that the length of the groove has the least impact on the evaporation rate. Therefore, it cannot be directly concluded that a longer the length of the groove always improves the evaporation rate. Based on the orthogonal analysis, the optimal choice is A3B1C3, corresponding to option g.

Performance comparison between traditional straight evaporator tube and new evaporator tube

Using the same model and boundary conditions, numerical simulations were conducted for a conventional straight evaporator tube without grooves, labeled as scheme j, and compared with the optimal scheme g obtained from the orthogonal experiments. The comparison results are presented in Table 5 and Figs. 7, 8, and 9. Data analysis reveals that the evaporation rate of the conventional tube is only 1.1%, whereas it increases significantly to 23.98% in scheme g due to the introduction of the innovative parallel-vein wall structure. This demonstrates the substantial performance enhancement achieved through structural optimization.

Programmatic	A	B	C	Evaporation rate(%)
a	1	1	1	18.01
b	1	2	2	3.01
c	1	3	3	3.92
d	2	1	2	6.79
e	2	2	3	2.37
f	2	3	1	2.50
g	3	1	3	23.98
h	3	2	1	2.58
i	3	3	2	5.20
K1	24.94	48.78	23.09	-
K2	11.66	7.96	15	-
K3	31.76	11.62	30.27	-
k1	8.31	16.26	7.70	-
k2	3.89	2.65	5	-
k3	10.59	3.87	10.09	-
Range	6.7	13.61	5.09	
Optimal solution	A3	B1	C3	

Table 4. Orthogonal experiment analysis table.

Programmatic	Evaporation rate(%)	Outlet SMD (μm)	Air flow (g/s)	Average outlet temperature(K)
e	23.98	29.52	2.551	539.93
j	1.1	35.91	2.554	511.15

Table 5. Comparison and analysis of calculation results between traditional and new evaporator tubes.

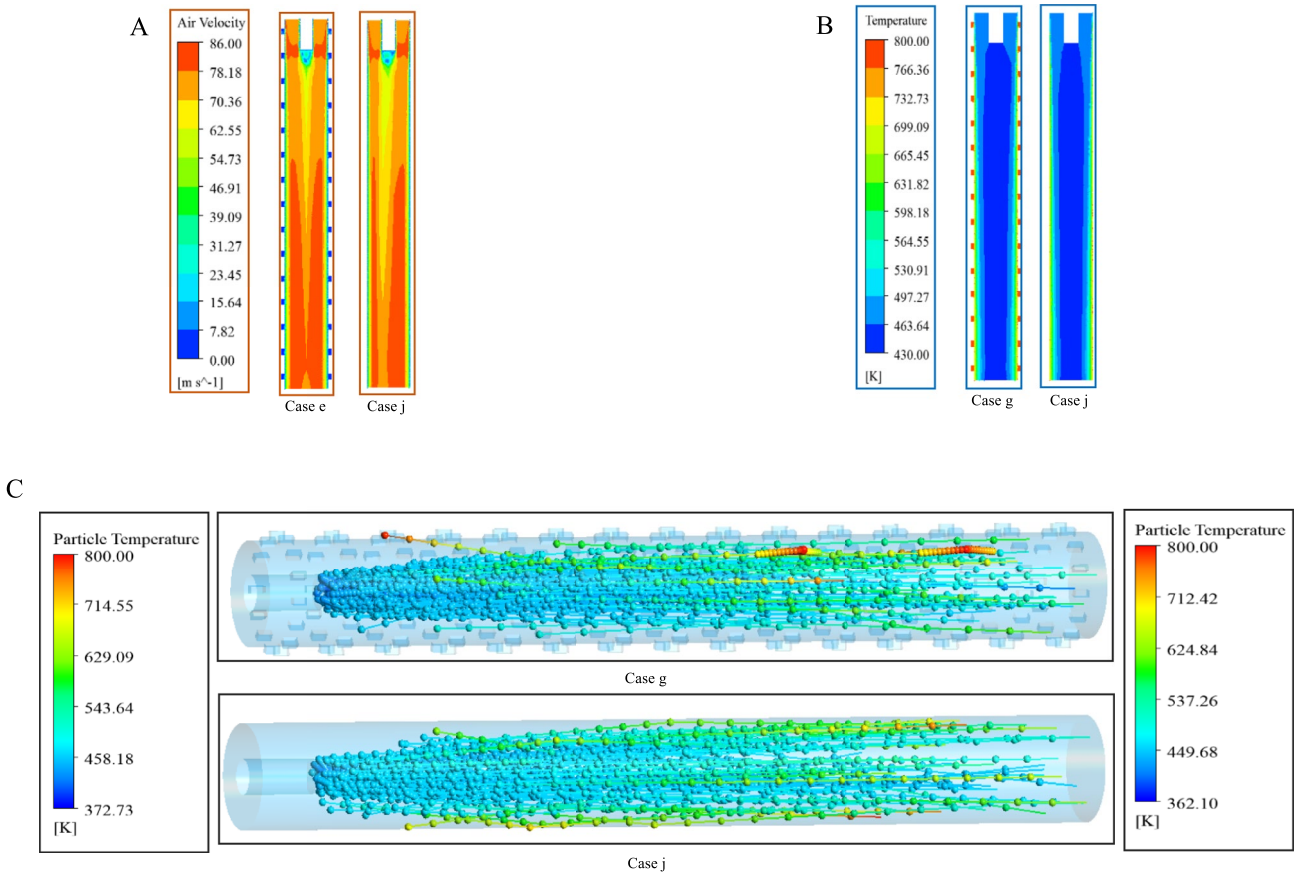

Fig. 10. Comparison between traditional and new models. (**A**) Comparison of velocity fields, (**B**) Comparison of temperature fields. (**C**) Comparison of temperature distribution of fuel droplets

Additionally, the Sauter mean diameter (SMD) of fuel droplets at the outlet is reduced from 35.91 μm to 29.52 μm, confirming the structure's effectiveness in promoting atomization. Meanwhile, the mean outlet temperature rises from 511.15 K to 539.93 K, indicating improved heat exchange efficiency between the tube wall and airflow, which accelerates droplet evaporation.

Although the new structure introduces some internal flow resistance, leading to a slight reduction in airflow under the same pressure differential, the decrease from scheme j to scheme g is minimal—from 2.554 g/s to 2.551 g/s—only 0.117%, and thus negligible.

From the perspective of combustion chamber design, maintaining a stable airflow rate based on a conventional straight-tube structure, while keeping other structural parameters unchanged, indicates that the implemented optimization measures are both effective and feasible. Airflow stability is critical for ensuring complete fuel combustion, stable operation, and overall system efficiency. The optimized structure in this study not only enhances heat transfer and evaporation but also maintains high airflow efficiency, enabling stable and efficient air supply.

This demonstrates that, even with a traditional design foundation, fine-tuning and localized structural improvements can enhance overall performance without compromising airflow. Such optimization, achieved without altering the key parameter of airflow, minimizes design-induced uncertainty and ensures the combustion chamber's operational stability and reliability—laying a solid foundation for developing more efficient and low-emission combustion systems.

As shown in Fig. 10, the air temperature inside the tube gradually increases along the flow direction. In terms of atomization, both the traditional and the new evaporator tubes exhibit low flow resistance, allowing air to

flow smoothly at high velocity. The airflow velocity distribution in both designs is generally uniform, ensuring overall flow stability.

However, the new evaporator tube, incorporating a parallel pulse wall structure, introduces significant disturbances to the incoming airflow while maintaining overall flow stability. This structural design notably alters the flow dynamics. Specifically, the enhanced internal geometry effectively guides and regulates the airflow path and velocity distribution. As a result, localized regions with steep velocity gradients—referred to as 'hot spots'—are formed within the tube. These areas intensify gas–liquid interactions by increasing the relative velocity between the phases, thereby enhancing the aerodynamic forces acting on fuel droplets. This facilitates droplet breakup and promotes more effective atomization.

The strengthened aerodynamic effects not only accelerate droplet fragmentation but also improve droplet refinement, leading to a significant improvement in overall atomization and evaporation performance. Thus, the structural optimization of the new evaporator tube markedly improves airflow characteristics and provides robust support for a more efficient atomization process.

In the internal structure of a conventional evaporator tube, as shown in scheme j, the high-temperature region gradually extends along the thickness of the tube wall, with the temperature steadily increasing. This phenomenon illustrates the path of heat propagation inside the tube and the extent of its influence. However, despite the crucial role of the tube wall in transferring heat to the external environment, its heat transfer efficiency is somewhat limited. Heat transfer primarily occurs in the air region close to the tube wall, causing the temperature in this area to rise. Most of the fuel droplets, however, are located in the center of the tube, away from the wall, where they are heated by the lower temperature air. As a result, their temperature increases more slowly, preventing them from reaching the evaporation point quickly and ultimately lowering the evaporation rate.

The new structural design offers two key advantages. First, the precisely engineered grooves in the tube wall disrupt the airflow, leading to an increase in the average temperature at the tube center and outlet, while significantly improving the uniformity of the temperature distribution. A more homogeneous temperature field ensures consistent thermal effects during evaporation, which enhances the atomization of fuel droplets. This uniformity promotes finer atomization and higher atomization efficiency. Additionally, the improved temperature uniformity accelerates the evaporation process, enabling faster and more complete conversion of fuel into vapor—critical for efficient combustion. Second, the grooved structure introduces a unique heat transfer pathway for the fuel droplets. As droplets travel through the tube, they collide with the grooves on the wall, increasing their contact area with the heated surface and enabling more effective direct heat exchange. Furthermore, the grooves guide the droplets into high-temperature regions along the wall, facilitating enhanced thermal interaction between the droplets and the surrounding hot air. This dual mechanism—direct heating from the wall and convective heating from the air—substantially boosts evaporation efficiency and accelerates the overall vaporization process.

As shown in Fig. 11A, the new evaporator tube with a parallel vein structure outperforms the conventional straight tube design across all scenarios. Notably, scheme g achieves the highest evaporation rate and the smallest Sauter Mean Diameter (SMD), clearly demonstrating its superior atomization and evaporation performance. Furthermore, Fig. 11B indicates that scheme g reaches the highest average outlet temperature with the lowest airflow rate, reflecting more efficient heat utilization. This enhanced performance is primarily attributed to the

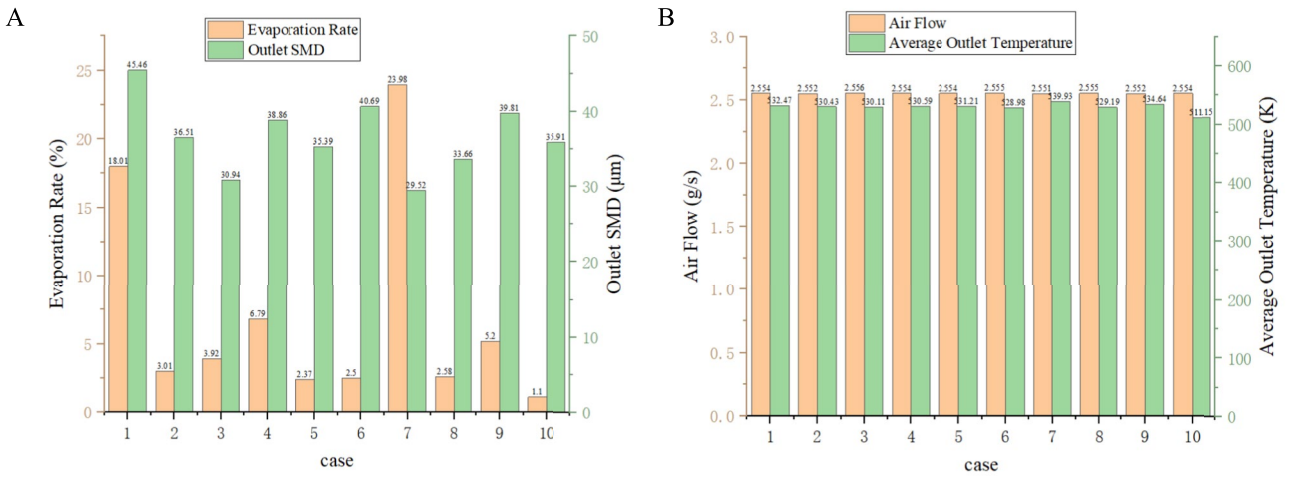

Evaporation rate and SMD outlet cross-section for each program

Air flow and average temperature outlet cross-section for each program

Fig. 11. Comparison of parameters between traditional and new Structures. (**A**) Evaporation rate and SMD outlet cross-section for each program, (**B**) Air flow and average temperature outlet cross-section for each program.

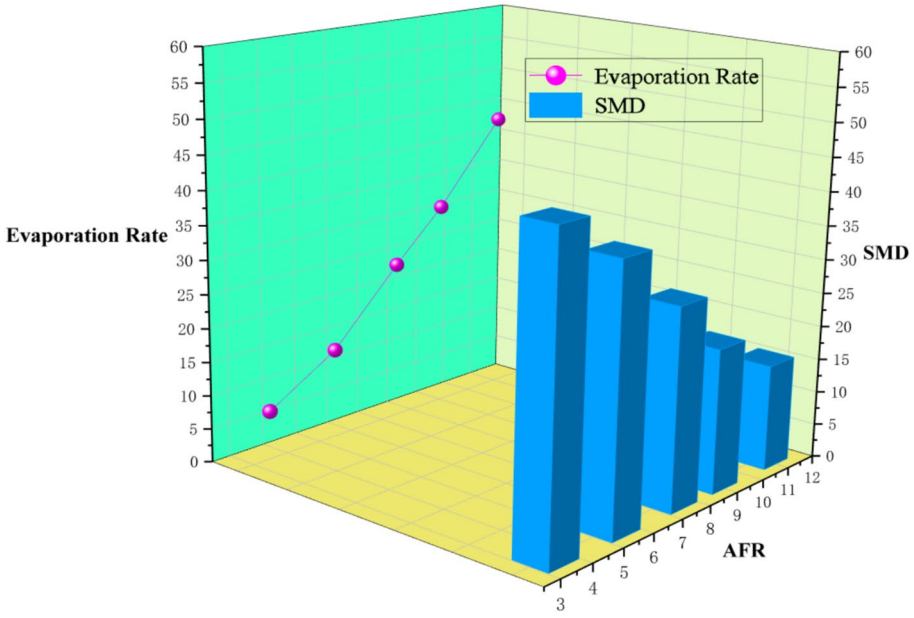

Fig. 12. The effect of gas oil ratio on evaporation performance.

innovative groove design on the parallel vein tube wall, which significantly improves heat exchange efficiency and optimizes heat distribution within the tube.

The influence of gas oil ratio on evaporation

Using the Air Fuel Ratio (AFR) inside the evaporator tube as a variable and a tube wall temperature of 800 K, this study investigates the impact of AFR on the fuel evaporation performance of the Scheme g evaporator tube. The calculation results, shown in Fig. 12, illustrate how changes in AFR influence the evaporation rate, droplet size, and overall performance of the fuel atomization process inside the evaporator tube.

The calculations are performed by keeping the pressure difference between the inlet and outlet of the evaporator tube constant, maintaining a steady air flow rate, and varying the fuel injection flow rate. As a result, the gas-to-oil ratio (AFR) changes within the range of 3.5 to 11, and the fuel flow rate varies from 0.233 g/s to 0.731 g/s. This setup allows for examining the influence of different AFRs on the fuel evaporation process within the Scheme G evaporator tube. This strategy focuses on simulating real operating conditions by maintaining a constant air flow rate while varying the fuel injection flow rate, thus adjusting the air–fuel ratio (AFR). This approach aims to reflect potential fuel supply fluctuations that occur in actual combustion chamber operations. By using this method, the study evaluates how these fluctuations impact the efficiency and atomization quality of the evaporator tube, providing insights into the stability and performance of the tube under realistic conditions. As the air–fuel ratio increases, the evaporation rate improves steadily, indicating that a higher gas-to-oil ratio enhances the evaporation process. This leads to more efficient fuel conversion into gas, which improves the overall preparation of the fuel before combustion. This trend highlights the importance of maintaining an optimal air–fuel ratio for efficient fuel atomization and combustion readiness in the evaporator tube. Precisely regulating the air–fuel ratio (gas-oil ratio) not only optimizes the evaporation efficiency of the evaporator tube but also significantly enhances the atomization process. A reduced Sauter mean diameter (SMD) indicates finer, more evenly distributed droplets, which improves combustion efficiency and reduces emissions. This highlights the critical role of controlling the gas-oil ratio in optimizing both fuel evaporation and atomization, contributing to a more stable and efficient combustion process.

Conclusion

This article presents the design of a novel evaporator tube structure inspired by the biomimetic characteristics of parallel leaf veins. It establishes a flow field and fuel evaporation model to investigate the fuel atomization and evaporation processes within the evaporator tube. The study analyzes the impact of various leaf vein parameters on fuel atomization and evaporation efficiency in a single evaporator tube, and draws the following conclusions:

(1) The width of the groove on the inner wall of the tube is a key factor influencing fuel atomization and evaporation. A narrower the width of the groove promotes increased turbulence, finer fuel particles, and improved atomization uniformity, enhancing the contact area, accelerating heat exchange, and promoting evaporation. This results in improved combustion efficiency and reduced emissions. However, if the width of the groove is too narrow, it may increase flow resistance, pressure loss, and processing difficulty, potentially affecting system stability and economic performance. In this study, the width of the groove of 0.5 mm is found to be optimal, as it yields better evaporation performance for fuel droplets.

(2) The depth of the groove on the inner wall of the tube significantly affects the fluid dynamics, thereby impacting the atomization and evaporation process of fuel droplets. As the depth of the groove increases, it can alter the flow path and velocity distribution of the fluid, which in turn affects the incoming flow velocity. This change in flow velocity directly influences the interaction between fuel droplets and the airflow, thereby affecting atomization quality and evaporation efficiency. A moderate the depth of the groove can enhance fluid turbulence, improve gas–liquid mixing, and promote better atomization. However, excessively deep grooves may increase fluid resistance, reduce flow velocity, and hinder atomization and evaporation. In this study, the depth of the groove of 0.6 mm is selected, as it provides the best evaporation performance.

(3) The length of the groove on the inner wall of the tube can trigger a series of chain reactions that significantly influence fuel atomization and evaporation. As the length of the groove increases, the contact time between the fluid and the groove wall is extended, which not only increases the likelihood of fluid disturbance and shear but also enhances heat exchange. This improved interaction facilitates more effective dispersion of fuel droplets into smaller particles, achieving finer atomization and accelerating the evaporation rate, thereby improving combustion efficiency. However, longer the length of the groove may also present challenges, such as increased fluid flow complexity, which could lead to higher pressure loss and flow resistance, potentially threatening the stability and efficiency of the fuel supply system. In the simulation experiments conducted in this study, the length of the groove of 1.5 mm resulted in the best evaporation performance.

Data availability

The datasets used and/or analysed during the current study available from the corresponding author on reasonable request.

Received: 3 March 2025; Accepted: 8 August 2025
Published online: 20 August 2025

References

1. Lyu, M. T., Li, F., Xu, G. Y. & Han, S. Leveraging eye-tracking technologies to promote aviation safety-A review of key aspects, challenges, and future perspectives. *Saf. Sci.* **168**(2), 106295–106322. https://doi.org/10.1016/j.ssci.2023.106295 (2023).
2. Shao, L. T. et al. Advanced combustion in heavy fuel aircraft piston engines: A comprehensive review and future directions. *Fuel* **370**(1), 131771–131792. https://doi.org/10.1016/j.fuel.2024.131771 (2024).
3. Teixeira, A., Silva, A., Cavalcante, R. & Young, A. Process simulation and economic evaluation of the Alcohol-to-Jet production of sustainable aviation fuel in the Brazilian context. *Energy Convers. Manage.* **2024**(319), 118947–118959. https://doi.org/10.1016/j.enconman.2024.118947 (2024).
4. Tiwari, S., Pekris, M. & Doherty, J. A review of liquid hydrogen aircraft and propulsion technologies. *Int. J. Hydrogen Energy* **57**(1110), 1174–1196. https://doi.org/10.1016/j.ijhydene.2023.12.263 (2024).
5. Niu, X. J., Liu, Z. W., Chen, Q. J. & Zhang, T. S. Determining the MEMS INS initial heading using trajectory matching for UAV applications. *IEEE Sens. J.* **24**(1), 543–553. https://doi.org/10.1109/JSEN.2023.3333383 (2023).
6. Wu, X. H. et al. An analysis approach for micro gas turbine engine's performance by experiment and numerical simulation. *Case Stud. Thermal Eng.* **49**(1), 103305–103319. https://doi.org/10.1016/j.csite.2023.103305 (2023).
7. Oni, B., Sanni, S., Ibegbu, A. & Tomomewo, O. Evaluation of engine characteristics of a micro-gas turbine powered with JETA1 fuel mixed with afzelia biodiesel and dimethyl ether (DME). *Renew. Energy* **216**(69), 119134–119143. https://doi.org/10.1016/j.renene.2023.119134 (2023).
8. Boretti, A. Towards hydrogen gas turbine engines aviation: A review of production, infrastructure, storage, aircraft design and combustion technologies. *Int. J. Hydrogen Energy* **88**(10), 279–288. https://doi.org/10.1016/j.ijhydene.2024.09.121 (2024).
9. Afonso, F. et al. Strategies towards a more sustainable aviation: A systematic review. *Prog. Aerosp. Sci.* **137**(5), 100878–100932. https://doi.org/10.1016/j.paerosci.2022.100878 (2023).
10. Ajaj, R., Parancheerivilakkathil, M. S., Amoozgar, M., Friswell, M. & Cantwell, W. Recent developments in the aeroelasticity of morphing aircraft. *Prog. Aerosp. Sci.* **120**(1), 100682–100710. https://doi.org/10.1016/j.paerosci.2020.100682 (2021).
11. Yang, B., Hu, L. B., Ping, W. W., Roy, R. S. & Gupta, A. Boron-nitride Nanosheet-based thermal barrier coating for Micro-combustor performance improvement. *J. Energy Res. Technol.* **144**(6), 062106–062109. https://doi.org/10.1115/1.4052734 (2021).
12. Clarke, J. S. & Jackson, S. R. General consideration in the design of combustion chambers for aircraft and industrial gas turbines. *Sae World Congress Exhib. Sydney Aus.* https://doi.org/10.4271/640009 (1964).
13. Zhao, R. B. et al. A dynamic control strategy for improving combustion chamber sweep efficiency during the in-situ combustion. *Appl. Therm. Eng.* **235**(11), 121439–121452. https://doi.org/10.1016/j.applthermaleng.2023.121439 (2023).
14. Zhao, M. H. et al. Numerical study on the flow characteristics and stability in the isolator of rotating detonation ramjet engine by different combustion modes and structure parameters. *Aerosp. Sci. Technol.* **147**(9), 108982–108995. https://doi.org/10.1016/j.ast.2024.108982 (2024).
15. Tang, Y. Z. et al. Effects of ignition methods and control parameters on the lean combustion performance and flame geometry of jet ignition based on constant-volume combustion chamber. *Energy Convers. Manage.* **309**(9), 118427–118440. https://doi.org/10.1016/j.enconman.2024.118427 (2024).
16. Tan, W. L., Fan, W. J., Zhang, T., Wang, W. J. & Zhang, R. C. Performance test of micro turbojet engines evaporator and numerical simulation of the combustor. *J. Aerospace Power* **27**, 861–867. https://doi.org/10.13224/j.cnki.jasp.2012.04.022 (2012).
17. Zhang, X. M., Zhang, Q. Y., Li, G. W. & Hu, J. Numerical study on atomization characteristics of biomimetic evaporation tube in micro turbine engine. *Iscience* **27**(3), 109144–109159. https://doi.org/10.1016/j.isci.2024.109144 (2024).
18. Peng, J. L., Fan, W. J. & Zhang, R. C. A study on liquid film and evaporation characteristics of fuel jet impingement on the scorching wall of evaporation tube for gas turbine. *Phys. Fluids* **36**(9), 93308–93327. https://doi.org/10.1063/5.0224737 (2024).
19. Xu, X. Y. et al. Bionic optimization for cooling structure of GaN HEMTs inspired by leaf vein structure. *Case Stud. Thermal Eng.* **53**(1), 103945–103961. https://doi.org/10.1016/j.csite.2023.103945 (2023).
20. Peng, G. Q. et al. Leaf venation architecture in relation to leaf size across leaf habits and vein types in subtropical woody plants. *Front. Plant Sci.* **13**(5), 873036–873049. https://doi.org/10.3389/fpls.2022.873036 (2022).
21. Zeng, S. T., Zhang, R. S. & Cai, Y. F. Research on digital morphogenesis and sustainability of 3D printing bionic materials based on convolutional neural networks. *IEEE Access* **12**(1), 80418–80428. https://doi.org/10.1109/ACCESS.2024.3410115 (2024).
22. Du, T. T., Ling, X. X., Huang, J. L., Peng, S. B. & Xiong, D. L. Photosynthesis of rice leaves with a parallel venation is highly tolerant to vein severing. *Physiol. Plant.* **176**(2), 14241–14253. https://doi.org/10.1111/ppl.14241 (2024).
23. Zhu, S. P., Zhang, Z. L., Chen, H. S. & Li, Y. Numerical investigation of a bionic vapor chamber based on leaf veins for cooling electronic devices. *Ustainability* **15**(2), 1125–1142. https://doi.org/10.3390/su15021125 (2023).

24. Bahn, C. B. & Oh, Y. J. Ligament rupture and unstable burst behaviors of axial flaws in steam generator U-bends. *Nucl. Eng. Des.* **293**(11), 228–237 (2015).
25. Muzaffar, A., Abbas, A., Cremaschi, L., Ayub, Z. & Cheema, T. Experimental study of two-phase pressure-drop in 180° horizontal return bend and contiguous straight tubes with ammonia (RP-1683). *Sci. Technol. Built Environ.* **31**(2), 1–16. https://doi.org/10.1080/23744731.2025.2452142 (2025).
26. Zhou, Z. H., Wang, X. & Zhou, Y. M. Performance study of a Leaf-vein-like structured vapor chamber. *Materials* **16**(12), 4482–4496. https://doi.org/10.3390/ma16124482 (2023).
27. Chen, J. J. et al. Experimental study of dielectric liquid spray cooling on multi-scale structured surfaces inspired by leaf veins. *Int. J. Heat Fluid Flow* **109**(10), 109554–109566. https://doi.org/10.1016/j.ijheatfluidflow.2024.109554 (2024).
28. Zhang, K. P. CFD simulation and experimental verification for one subway air-conditioning condensing unit. *Refriger. Air-Condition.* **19**(10), 45–49 (2019).

Acknowledgements

This research is supported by the Jilin Natural Science Foundation of China under Contract No. 20240101103JC.

Author contributions

Q. Y., Z. collected data and wrote the article; X. M., Z. supervised the article and funding acquisition; J. H. conceived the idea、funding acquisition and visualization; G. W., L. analyzed data; and all authors discussed the results and approved the article.

Declarations

Competing interests

The authors declare no competing interests.

Additional information

Supplementary Information The online version contains supplementary material available at https://doi.org/10.1038/s41598-025-15621-5.

Correspondence and requests for materials should be addressed to X.Z. or J.H.

Reprints and permissions information is available at www.nature.com/reprints.

Publisher's note Springer Nature remains neutral with regard to jurisdictional claims in published maps and institutional affiliations.